minerals

MDPI

Article

Compositional Variations of Spinels from Ultramafic Lamprophyres of the Chadobets Complex (Siberian Craton, Russia)

Yazgul Nugumanova [1,2,*], Anna Doroshkevich [1,3], Ilya Prokopyev [1,2] and Anastasiya Starikova [1,2]

[1] Sobolev Institute of Geology and Mineralogy, Siberian Branch of the Russian Academy of Sciences, Akademika Koptyuga Avenue 3, 630090 Novosibirsk, Russia; doroshkevich@igm.nsc.ru (A.D.); prokop@igm.nsc.ru (I.P.); a_sklr@mail.ru (A.S.)
[2] Department of Geology and Geophysics, Novosibirsk State University, Pirogova Street 1, 630090 Novosibirsk, Russia
[3] Geological Institute, Siberian Branch of the Russian Academy of Sciences, Sakhyanova Street 6a, 670047 Ulan-Ude, Russia
* Correspondence: nugumanovayn@igm.nsc.ru; Tel.: +7-919-153-0889

Abstract: Ultramafic lamprophyres (UMLs) are mantle rocks that provide important information about the composition of specific carbonate–silicate alkaline melts in the mantle as well as the processes contributing to their origin. Minerals of the spinel group typically occur in UMLs and have a unique "genetic memory." Investigations of the spinel minerals from the UMLs of the Chadobets complex show the physicochemical and thermodynamic features of the alkaline rocks' crystallization. The spinels of these UMLs have four stages of crystallization. The first spinel xenocrysts were found only in damtjernite pipes, formed from mantle peridotite, and were captured during the rising of the primary melt to the surface. The next stages of the spinel composition evolution are related to the high-chromium spinel crystallization, which changed to a high-alumina composition. The composition then changed to magnesian ulvöspinel–magnetites with strong decreases in the Al and Cr amounts caused by the release of carbon dioxide, rapid temperature changes, and crystallization of the main primary groundmass minerals such as phlogopite and carbonates. Melt inclusion analyses showed the predominance of aluminosilicate (phlogopite, clinopyroxene, and/or albite) and carbonate (calcite and dolomite) daughter phases in the inclusions that are consistent with the chemical evolution of the Cr-spinel trend. The further evolution of the spinels from magnesian ulvöspinel–magnetite to Ti-magnetite is accompanied by the formation of atoll structures caused by resorption of the spinel minerals.

Keywords: ultramafic lamprophyre; aillikite; damtjernite; Chadobets upland; Siberian Craton; minerals of the spinel group; zoning; atoll spinel

Citation: Nugumanova, Y.; Doroshkevich, A.; Prokopyev, I.; Starikova, A. Compositional Variations of Spinels from Ultramafic Lamprophyres of the Chadobets Complex (Siberian Craton, Russia). *Minerals* **2021**, *11*, 456. https://doi.org/10.3390/min11050456

Academic Editors: Anna A. Nosova and Alexey V. Kargin

Received: 12 April 2021
Accepted: 23 April 2021
Published: 26 April 2021

1. Introduction

Ultramafic lamprophyres (UMLs) and kimberlites are deep mantle rocks that provide important information about the composition of carbonate–silicate alkaline melts, and their origin and classification are subjects of debate [1–10]. Usually, the formation of rocks is accompanied by the activity of late-stage fluids, causing silicate minerals to undergo hydrothermal alteration. Oxides, as more stable minerals, can be important indicators of the conditions under which the generation and evolution of kimberlites and ultrabasic lamprophyres occur and have a unique "genetic memory". Minerals of the spinel group are typical oxides found in kimberlites and UMLs. They include a wide range of natural compounds with the general formula AB_2O_4, where A indicates divalent cations (Mg^{2+}, Zn^{2+}, Mn^{2+}, Fe^{2+}, Co^{2+}, Ni^{2+}) occupying tetrahedral positions in the structure, and B includes trivalent cations (Al^{3+}, Fe^{3+}, Cr^{3+}, Mn^{3+}, V^{3+}) and Ti^{4+} occupying octahedral positions [11–16].

In kimberlites and UMLs, spinels are represented by groundmass minerals, crystallizing directly from the parental melt, and spinel macrocrysts and xenocrysts, formed during the destruction of mantle xenoliths and captured by the melt while rising to the surface [17–22]. These groups of spinels differ in composition and texture [17,18,23–26]. Moreover, groundmass spinels are formed under a wide range of physicochemical and thermodynamic conditions and are indicator minerals of the crystallization and evolution of rocks [18,27,28].

The UMLs (aillikites and damtjernites) of the Chadobets complex, located in the southern part of the Siberian Craton, were formed during the Permian–Triassic period of magmatic activity on the craton, accompanied by the formation of one of the largest trap basalt provinces, meimechites, kimberlites, and carbonatites. General information on the spinels of the Chadobets complex is presented in several publications [29–32], where the authors consider the similarity of their compositions to Group II kimberlites (orangeites).

This study presents the macro- and microcomponent compositions of minerals of the spinel group and their inclusions from the groundmass spinels of UMLs (aillikites and damtjernites) of the Chadobets complex to determine the main factors responsible for variations in the composition of spinels and the characteristics of the crystallization process of these rocks.

2. Geology and Petrography

The Chadobets alkaline complex of UMLs and carbonatites is located in the southern part of the Siberian Craton (Figure 1). Tectonically, it is confined to the large positive structure of the platform that is represented by the Chadobets dome-shaped uplift. The core of the uplift forms two protrusions, the northern Terina complex and southern Chuktukon complex, and is composed of carbonate–terrigenous Precambrian and early Cambrian sediments [13,30,33–36].

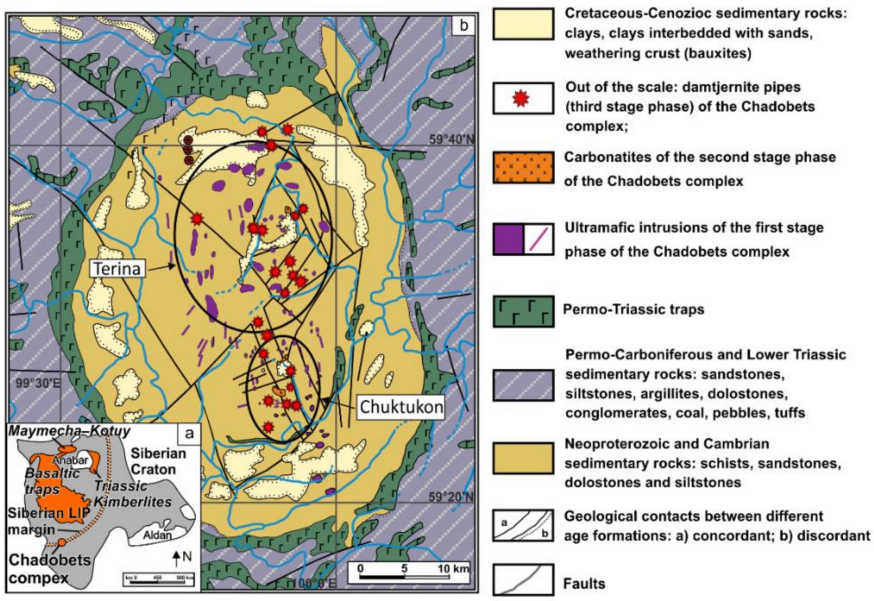

Figure 1. (**a**) Location of the Chadobets ultramafic lamprophyre (UML)–carbonatite complex within the Siberian Large Igneous Provence (LIP) on the Siberian Craton. (**b**) Geological scheme of the Chadobets alkaline complex [37].

The main intrusive rocks of the Chadobets complex are alkaline–ultramafic rocks (pyroxenites, aillikites, and damtjernites) and carbonatites [30]. The first phase of alkaline–ultramafic rocks forms stocks, dikes, and sills (Figure 1b). Carbonatites cut the first phase of alkaline rocks. The carbonatites form dikes and sills. Damtjernites consist of explosion tubes, have crosscutting contacts with the earlier alkaline phases, and contain xenoliths of these alkaline phases as well as fragments of sedimentary rocks [30]. The U–Pb

ages of the aillikites (perovskite) and damtjernites (zircon) give values of 252 ± 12 and 256.7 ± 1.1 Ma, respectively [29,38,39]. The Ar–Ar and Rb–Sr dates of the aillikites are 243 ± 3 and 241 ± 1 Ma [31].

The UMLs of the first phase of intrusion are aillikites and mela-aillikites and have a porphyritic structure; the proportion of phenocrysts varies from 20% to 50%. Macrocrysts are represented by idiomorphic grains of olivine (up to 20%), completely or partially replaced by serpentine and calcite. In olivines, the #Mg varies within grains, individual crystals, and their microcomponent compositions [40]. Phlogopite phenocrysts (up to 15–20 vol.%) have a zonal structure; often magnesian cores of #Mg 0.78–0.73 are overgrown with a ferrous rim of #Mg 0.47–0.12. The mineral composition of mela-aillikites differs from the aillikites in the presence of hypidiomorphic elongated clinopyroxene grains: diopside with an aegirine minal (up to 10%) [40]). The groundmass of UMLs contains predominant mineral phases of calcite, dolomite, and phlogopite, as well as disseminated micrograins of spinels, ilmenite, Ti-magnetite, apatite, and rare sulfides (chalcopyrite, pentlandite, etc.).

The ore-bearing rare-earth–niobium carbonatites of the Chadobets complex are fine- and medium-grained rocks with a massive and banded structure. Calcite is the predominant mineral in the groundmass (up to 95–98%). The most common non-carbonate minerals are tainiolite, fluorapatite, and fluorocalciopyrochlore [38]. Rippite, fluorite, Nb-rutile, potassium feldspar, aegirine, ancylite-(Ce), strontianite, sulfides, and zircon are minor and accessory mineral phases in the carbonatites. Barite, quartz, goethite, carbonate–fluorapatite–REE and Ca–REE–fluorocarbonates, parisite-(Ce), synchisite-(Ce), monazite-(Ce), hydropyrochlore, and romaneshite–hollandite minerals also represent hydrothermal mineralization. The carbonatites underwent strong hydrothermal alterations and subsequent weathering to form the Nb-ores [38].

Damtjernites of the third phase of intrusion of the Chadobets complex have porphyritic and usually brecciated structures and differ by the presence of hypidiomorphic feldspar grains of potassium feldspar and albite (up to 10%) in the groundmass, as well as in the pelletal lapilli (more than 60%). The pelletal lapilli of damtjernites contain macrocrysts of olivine, which are completely replaced by serpentine and calcite, and include magnetite, biotite, and a fine-grained aggregate of chlorite, serpentine, calcite, and quartz. The groundmass of the damtjernites contains phlogopite, dolomite, clinopyroxene, potassium feldspar, albite, microphenocrysts of Cr-spinels with a rim of Ti-magnetite, perovskite, and apatite [29,40].

3. Materials and Methods

The analytical works were performed using the facilities of the Analytical Center for Multi-Elemental and Isotope Research at the V.S. Sobolev Institute of Geology and Mineralogy (Novosibirsk, Russia). The analyses were performed on spinel grains from UMLs. These grains were collected from the exploratory drill cores of the Chuktukon complex and outcrop samples from the Terina riverbanks.

Polished rock samples were prepared for study in reflected light under a polarizing microscope (Olympus BX51) with a photo camera device. The polished rock samples were used to determine the rock textures and mineral assemblage compositions using energy-dispersive spectrometry in combination with back-scattered electron imaging (BSE) using the TESCAN MIRA 3 LMU JSM-6510LV scanning electron microscope with the energy prefix from X-Max Oxford Instruments for microprobe analysis. Pure cobalt was used as a calibration standard. All samples for inclusion study were hand polished in dry conditions with diamond pastes, using benzene or alcohol to preserve water-soluble phases in the inclusions.

The microcomponent composition of spinels was determined using a JEOL JXA-8230 electron microprobe. The analysis was carried out on spectrometers with wave dispersion. To analyze minerals of the spinel group, we used a beam current of 50 nA and an accelerating voltage of 20 kV. Peak counting time was 10 s; background counting was 5 s. The beam diameter directly above the sample surface was 1 μm. Both natural minerals

and synthetic phases were used as standards for calibration (element, standard, detection limits in ppm): Mg (79–62 (natural chromite from the Yakutia pipe); 496 ppm), Fe (Fe_2O_3 (synthetics); 402 ppm), Mn (IGEM (natural Mu-Grt from IGEM); 294 ppm), Zn ($ZnFe_2O_4$ (synthetics); 504 ppm), Ti (Gf-55 (ilmenite); 182 ppm), Al (79–62; 242 ppm), Si (IGEM; 240 ppm), Cr (79–62; 292 ppm), Ni (NiFe2O4 (synthetics); 239 ppm), Co (FeNiCo (alloy); 219 ppm), V (V_2O_5 (synthetics); 292 ppm).

Basic element oxides (wt%) were converted to the number of cations per atom per formula unit (apfu), in accordance with the recommendations in the appendix to Deer et al. (2013) [16]. The proportion of Fe^{2+} and Fe^{3+} was calculated assuming spinel stoichiometry [41]. In zonal spinels of different composition, the zones were distinguished using contrast during visualization of BSE images, elemental X-ray images, and linear profiles.

4. Results

Spinels are widespread in the groundmass of the studied rocks. The grain size varies within a range of 10–300 µm. Idiomorphic and subidiomorphic crystals are typical; grains with atoll texture were also found (Figure 2). Spinel grains can be both homogeneous and heterogeneous (zonal) according to their chemical compositions. We have identified the following types of spinels: Cr-spinels (Cr-Spl), Cr-magnetites (Cr-Mgt), Ti-magnetites (Ti-Mgt), magnetites (Mgt), magnesian ulvöspinel–magnetites (Mum), and aluminum spinel (Al-Spl) (Figure 2, Table 1). According to the endmember classification of spinels by [41] Cr-spinel series is represented by Al-rich chromite ($FeCr_2O_4$) and magnesiochromite ($MgCr_2O_4$). Cr-magnetite belongs to a series of ferrous spinels with a high chromium content. Al-spinel series is represented by Cr-rich spinel ($MgAl_2O_4$) and hercynite ($FeAl_2O_4$).

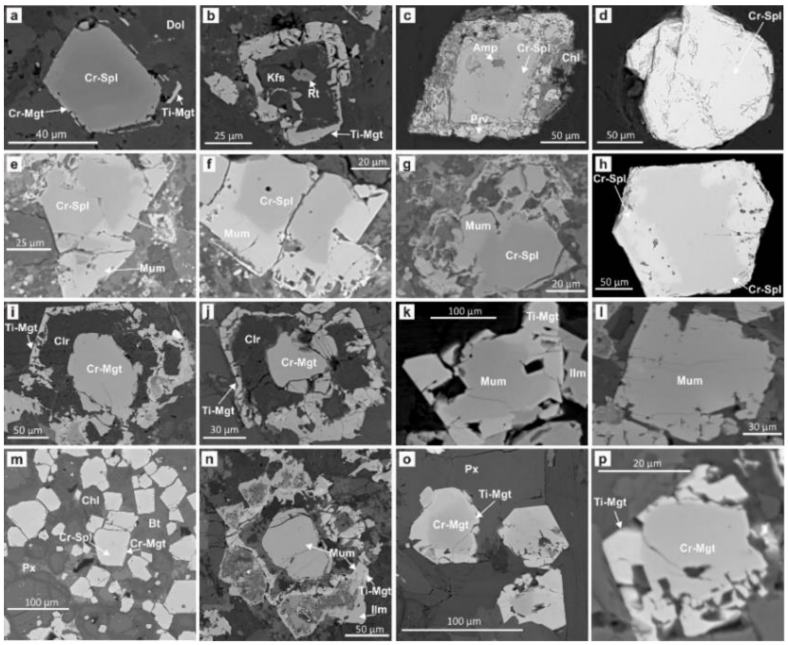

Figure 2. BSE images of minerals of the spinel group from Terina aillikites (**i**–**p**); Chuktukon damtjernites (**a**–**d**,**h**) and aillikites (**e**–**g**). Cr-Spl—chrome spinel, Cr-Mgt—Cr-magnetite, Mum—magnesio-ulvospinel-magnetite, Mgt—magnetite, Ti-Mgt—titanomagnetite, Dol—dolomite, Px—pyroxene, Prv—perovskite, Bt—biotite, Kfs—potassium feldspar, Rt—rutile, Amp—amphibole, Chl—chlorit.

Table 1. Representative chemical composition of the spinel group minerals from the Chdobets ultramafic lamprophyres.

Complex	**Chuktukon**										**Terina**							
Rock	**Damtjernites**			**Aillikites**							**Damtjernites**				**Aillikites**			
Type	**Cr-Spl**	**Cr-Spl**	**Cr-Spl**	**Cr-Spl**	**Cr-Spl**	**Al-Spl**	**Al-Spl**	**Mum**	**Mum**	**Mum**	**Cr-Spl**	**Cr-Spl**	**Cr-Mgt**	**Cr-Mgt**	**Mum**	**Mum**	**Cr-Spl**	**Cr-Spl**
Variety [41]	**Mg-Chr**	**Chr**	**Chr**	**Mg-Chr**	**Mg-Chr**	**Spl**	**Spl**	**Mgt**	**Mgt**	**Mgt**	**Chr**	**Chr**	**Mgt**	**Mgt**	**Mgt**	**Mgt**	**Chr**	**Chr**
wt%																		
SiO_2	0.00	0.24	0.00	0.00	0.00	0.00	0.00	0.00	0.00	0.00	0.00	0.00	0.30	0.00	0.00	0.00	0.00	0.00
TiO_2	3.17	4.34	5.37	2.82	4.25	5.10	6.51	16.03	17.65	16.01	7.82	7.82	10.61	9.94	13.36	14.93	10.04	10.14
Al_2O_3	18.74	12.87	13.09	20.01	20.18	20.10	17.74	8.16	3.21	3.25	8.31	8.31	6.93	8.01	3.16	3.50	8.41	7.33
Cr_2O_3	38.21	39.07	35.52	38.54	30.31	24.58	20.55	1.02	0.32	0.00	28.95	28.95	17.39	20.55	0.00	0.00	22.89	22.03
V_2O_3	0.00	0.00	0.00	0.00	0.00	0.00	0.00	0.00	0.00	0.00	0.00	0.00	0.00	0.00	0.00	0.00	0.00	0.00
Fe_2O_3	7.94	10.13	12.72	7.37	11.70	14.33	18.45	33.05	35.27	38.11	18.01	18.01	26.47	23.44	42.05	40.34	20.50	22.93
FeO	18.14	21.80	22.09	17.39	18.57	19.05	20.91	29.63	37.16	37.32	25.10	25.10	28.51	27.48	33.53	33.00	26.92	25.99
MgO	12.57	10.48	10.83	12.95	12.84	12.54	11.96	11.14	6.90	5.77	9.32	9.32	9.15	9.15	6.22	7.79	9.60	9.83
NiO	0.36	0.37	0.00	0.45	0.00	0.00	0.00	0.00	0.00	0.00	0.00	0.00	0.00	0.00	0.00	0.00	0.00	0.00
Total	99.13	99.29	99.62	99.54	97.84	95.70	96.12	99.03	100.51	100.46	97.50	97.50	99.36	98.57	98.32	99.56	98.36	98.25
Formulae based on 3 cations and 4 atoms of oxygen, apfu																		
Si	0.000	0.008	0.000	0.000	0.000	0.000	0.000	0.000	0.000	0.000	0.000	0.000	0.010	0.000	0.000	0.000	0.000	0.000
Ti	0.076	0.107	0.132	0.066	0.102	0.125	0.163	0.410	0.472	0.412	0.204	0.204	0.273	0.256	0.355	0.439	0.257	0.260
Al	0.706	0.496	0.505	0.739	0.756	0.772	0.696	0.327	0.134	0.131	0.340	0.340	0.280	0.323	0.131	0.161	0.338	0.294
Cr	0.966	1.011	0.920	0.955	0.761	0.633	0.541	0.027	0.009	0.000	0.793	0.793	0.471	0.556	0.000	0.000	0.616	0.593
V	0.000	0.000	0.000	0.000	0.000	0.000	0.000	0.000	0.000	0.000	0.000	0.000	0.000	0.000	0.000	0.000	0.000	0.000
Fe^{3+}	0.191	0.250	0.314	0.174	0.280	0.351	0.462	0.845	0.943	0.981	0.470	0.470	0.682	0.604	1.117	1.187	0.526	0.587
Fe^{2+}	0.485	0.597	0.605	0.456	0.493	0.519	0.582	0.842	1.104	1.067	0.728	0.728	0.816	0.787	0.990	1.079	0.767	0.740
Mg	0.599	0.511	0.529	0.605	0.608	0.609	0.594	0.564	0.365	0.294	0.482	0.482	0.467	0.467	0.327	0.454	0.487	0.499
Ni	0.009	0.010	0.000	0.011	0.000	0.000	0.000	0.000	0.000	0.000	0.000	0.000	0.000	0.000	0.000	0.000	0.000	0.000
Calculated parameters																		
Mg#	0.55	0.46	0.47	0.57	0.55	0.54	0.50	0.40	0.25	0.22	0.40	0.40	0.36	0.37	0.25	0.30	0.39	0.40
Cr#	0.58	0.67	0.65	0.56	0.50	0.45	0.44	0.08	0.06	0.00	0.70	0.70	0.63	0.63	0.00	0.00	0.65	0.67
Ti#	0.04	0.07	0.08	0.04	0.06	0.08	0.12	0.54	0.77	0.76	0.15	0.15	0.27	0.23	0.73	0.73	0.21	0.23
Fe^{2+}#	0.45	0.54	0.53	0.43	0.45	0.46	0.50	0.60	0.75	0.78	0.60	0.60	0.64	0.63	0.75	0.70	0.61	0.60
Fe^{3+}#	0.10	0.14	0.18	0.09	0.16	0.20	0.27	0.70	0.87	0.88	0.29	0.29	0.48	0.41	0.89	0.88	0.36	0.40

Mg# = Mg/(Mg + Fe^{2+}); Cr# = Cr/(Cr + Al); Ti# = Ti/(Ti + Cr + Al); Fe^{2+}# = Fe^{2+}/(Fe^{2+} +Mg); Fe^{3+}# = Fe^{3+}/(Fe^{3+} +Cr + Al). Mg-Chr—magnesiochromite, Chr—chromite, Spl—spinel, Mgt—magnetite.

4.1. Terina Complex Spinels

In aillikites, zonal idiomorphic and subidiomorphic crystals with sizes of 20–100 μm (Figure 2) represent spinels. Cr-spinels are overgrown with Cr-magnetite or Cr-magnetite with magnesian ulvöspinel–magnetite (Mum), and Mum themselves are covered with a rim of Ti-magnetite (Figure 2i–p). Magnetites are also found in the form of separate subidiomorphic grains, 100–300 μm in size, and do not overgrow other types of spinels. Some samples contain atoll-textured spinels. The lagoon between the core and the rim is filled with chlorite, and the rim is composed of Ti-magnetite (Figure 3).

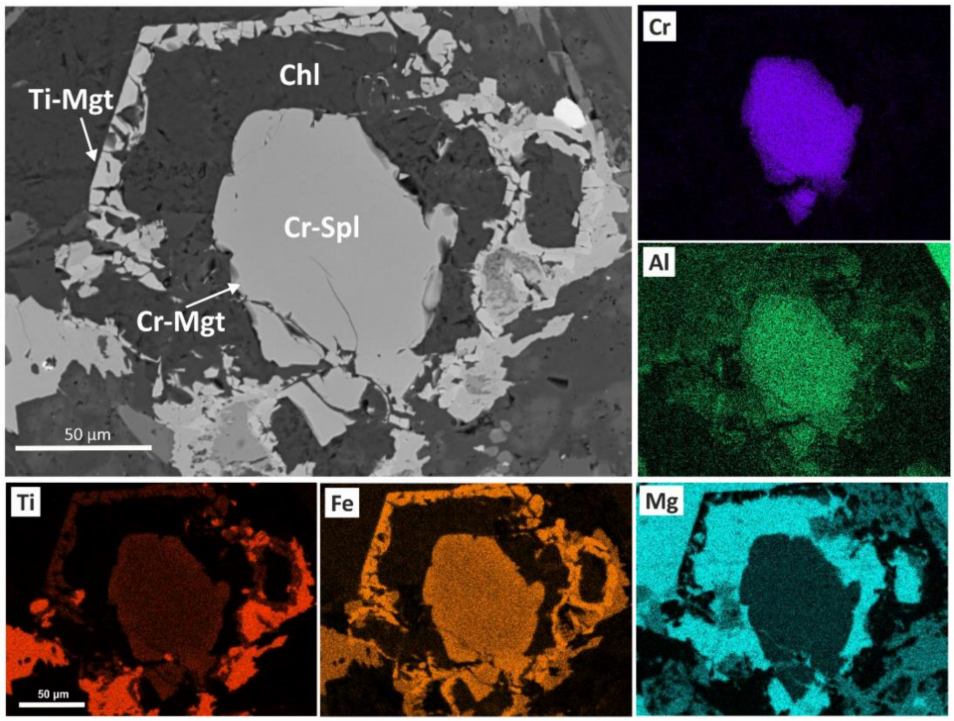

Figure 3. Atoll spinel from the aillikites of Terina, BSE images and electron microprobe (EMP) X-ray element maps.

In the aillikites, the following types of spinels were distinguished by their chemical compositions:

(1) Cr-spinels—$(Fe^{2+},Mg^{2+})\ (Cr,Fe^{3+},Al,Ti)_2O_4$;
(2) Cr-magnetites—$(Fe^{2+},Mg^{2+})\ (Fe^{3+},Cr,Ti,Al)_2O_4$;
(3) Mum—$(Fe^{2+},Mg^{2+})\ (Fe^{3+},Ti,Cr{\leftrightarrow}Al)_2O_4$;
(4) Ti-magnetites—$(Fe^{2+},\ Mg^{2+})\ (Fe^{3+},\ Ti,\ Al)_2\ O_4$.

In Cr-spinel, the content of Cr, Al, and Mg from the center of the grain to the edge decreases within the range 0.727 → 0.589 phase units (ph.u.) for Cr, 0.333 → 0.296 ph.u. for Al, and 0.491 → 0.488 ph.u. for Mg. There is an increase in Fe^{3+} of 0.505 → 0.587 ph.u., in Ti of 0.215 → 0.259 ph.u., and in Fe^{2+} of 0.722 → 0.757 ph.u. The Cr/(Cr + Al) ratio varies from 0.63 to 0.71.

The change in the composition of Cr-magnetites from the center to the edge of the grain shows a decrease in the content of Cr (0.494 → 0.407 ph.u.), Al (0.253 → 0.215 ph.u.), and Mg (0.488 → 0.464 ph.u.), and an increase in Fe^{3+} (0.622 → 0.721 ph.u.), Ti (0.307 → 0.323 ph.u.), and Fe^{2+} (0.811 → 0.857 ph.u.).

In Mum spinels, the content of Cr decreases (to 0.001 ph.u.), as does that of Al (to 0.1 ph.u.), from the center to the edge of the grain, whereas the contents of Fe^{2+} and Fe^{3+} increase. The contents of Ti and Mg do not change from the center to the periphery of the crystal. Ti-magnetites are enriched in Fe relative to Mum, and Cr is absent in their composition. The Al and Mg content drops to 0.01 ph.u. (Figure 4).

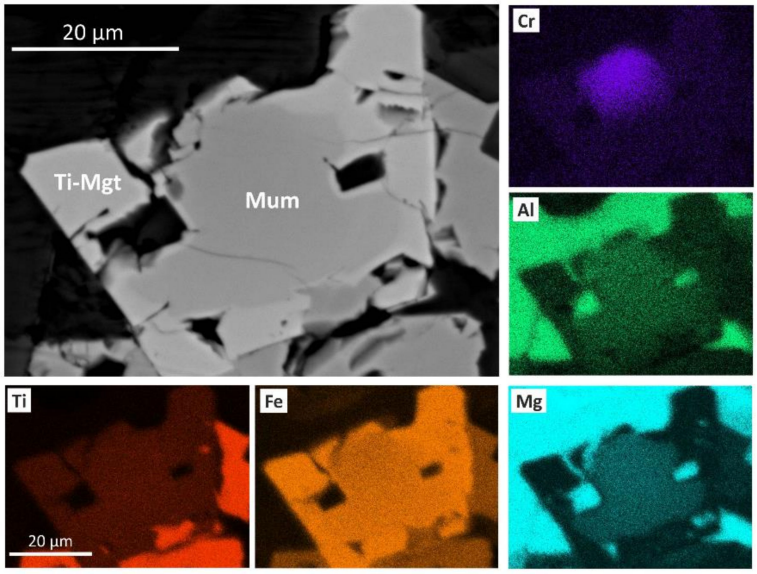

Figure 4. Mum and Ti-magnetite from the aillikites of Terina, BSE images and electron microprobe (EMP) X-ray element maps.

The main components of magnetites are Fe^{3+}, Fe^{2+}, and Ti (up to 0.2 ph.u.); the contents of Cr, Al, and Mg do not exceed 0.010 ph.u. In terms of the ratio of Fe, Ti, Cr, Al, and Mg, the spinels belong to the Ti-magnetite trend (Trend 2 according to Mitchell (1995)), which is characteristic of Type II kimberlites (orangeites) and UMLs (Figure 5).

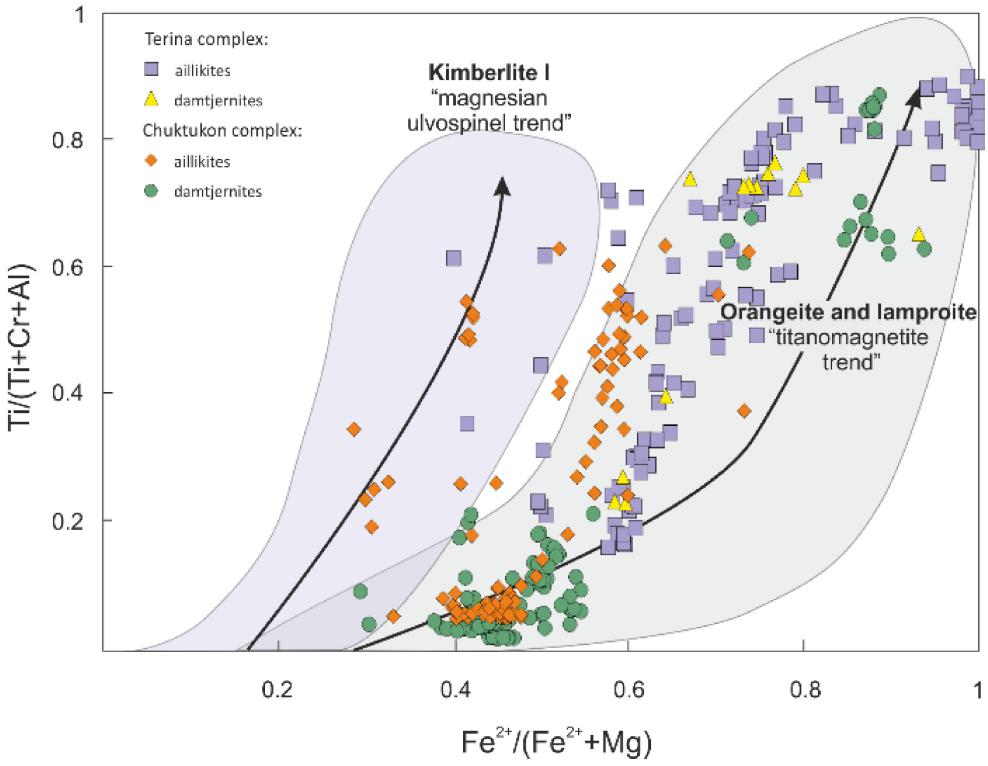

Figure 5. Plot of atomic ratios Ti/(Ti + Cr + Al) and $Fe^{2+}/(Fe^{2+}$ + Mg) for minerals of the spinel group [42].

The spinel analyses are plotted on a graph showing $Fe^{3+}/(Fe^{3+}$ + Al + Cr) vs. $Fe^{2+}/(Fe^{2+}$ + Mg) and on an Al–Fe^{3+}–Cr triangular diagram (Figure 6). In the aillikites, there is a continuous change in composition from Cr-spinel to Ti-magnetite (Trend 3), with a decrease

in the amount of Al and Cr and an increase in Fe. In Figure 7, it can be seen that from Cr-spinel to Ti-magnetite, there is a positive Mg–Cr correlation.

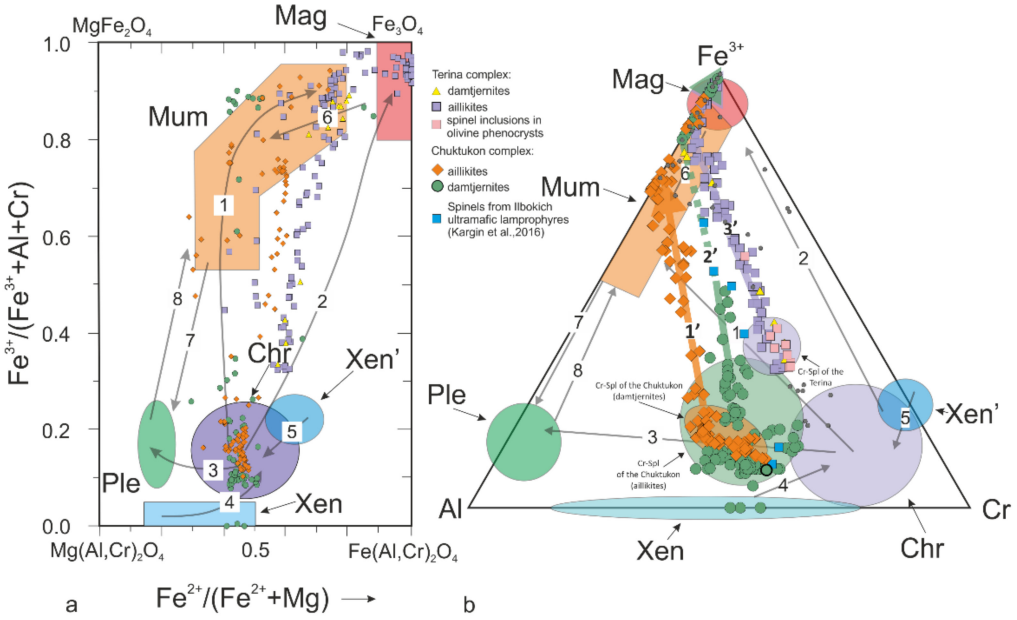

Figure 6. (**a**) Plot of $Fe^{3+}/(Fe^{3+} + Al + Cr)$ & $Fe^{2+}/(Fe^{2+} + Mg)$ and (**b**) diagram Al–Fe^{3+}-Cr. Xen—spinel xenocrystals from peridotites, Xen'—metasomatized spinel xenocrystal from peridotites, Chl—chromite, Ple—pleonast-spinel, Mum—magnesio-ulvospinel-magnetite and magnetite (Mag). The lines show possible evolutionary trends for different genetic types of spinels [27]. Black circles are the spinels from ultramafic lamphrophyres of Greenland and Canada [43–45].

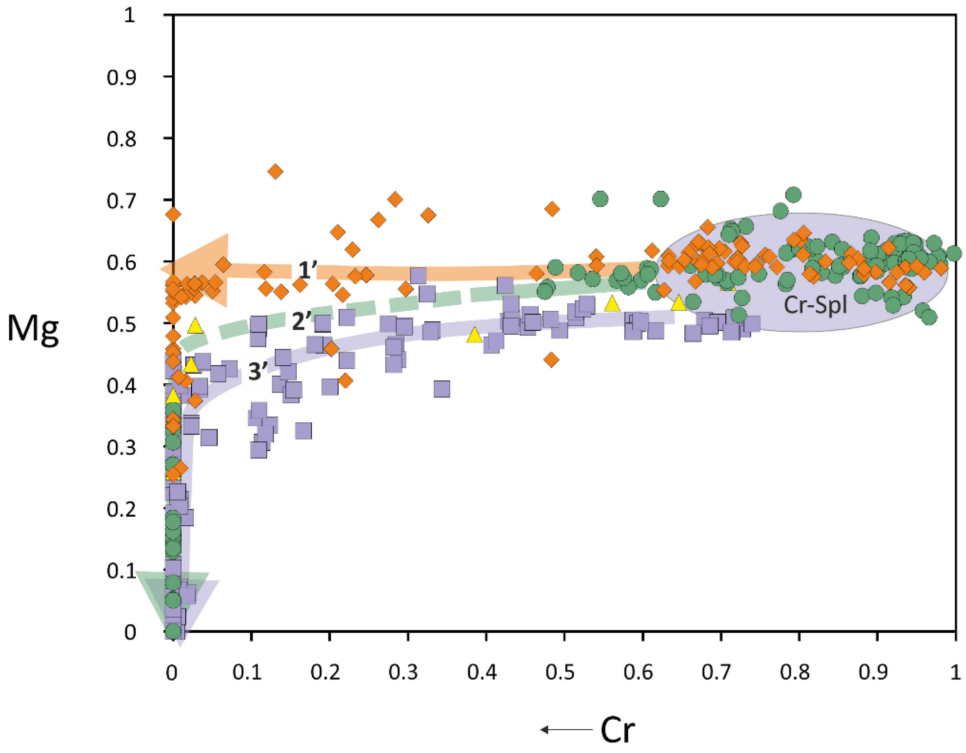

Figure 7. Plots of Mg (apfu) and Cr (apfu) for spinels from ultramafic alkaline rocks of the Chadobets complex. Symbols are as shown in Figure 6.

In aillikite spinels, the Mn content increases from 0.20 weight percent (wt%) in Cr-spinel to 0.90 wt% in Ti-magnetite. Variations in Zn (0.02–0.14 wt%) depend little on the contents of the main components (Cr, Al, Ti, Fe^{3+}). The V content is similar (0.10–0.40 wt%) between different types of spinel, but within the groups shows a significant change in content. In Cr-magnetites and Mum, the V content decreases from the center to the periphery of the grain, while the opposite trend is observed in Ti-magnetites. The content of Mn in Cr-spinel remains at the same level (0.25 wt%), while in Cr-magnetite it begins to increase and reaches a maximum in Ti-magnetite (0.52 wt%). Cr and Ni are closely related and behave in a similar manner.

In damtjernites, as in aillikites, the same types of spinels were identified:

(1) Cr-spinels—(Fe^{2+}, Mg^{2+}) ($Cr,Fe^{3+},Al,Ti)_2O_4$;
(2) Cr-magnetites—(Fe^{2+}, Mg^{2+}) ($Fe^{3+},Cr,Ti,Al)_2O_4$;
(3) Mum—(Fe^{2+}, Mg) ($Fe^{3+},Ti,Cr\leftrightarrow Al)_2O_4$;
(4) Ti-magnetites—(Fe^{2+}, Mg^{2+}) (Fe^{3+}, Ti, $Al)_2$ O_4.

Idiomorphic crystals with a size of 10–100 μm represent all types of spinels from damtjernites. In Cr-spinels, from the center of the grain to the edge, there is a decrease in the concentrations of Cr (0.780 → 0.645 ph.u.), Al (0.286 → 0.284 ph.u.), and Mg (0.565 → 0.534 ph.u.), and an increase in Fe^{3+} (0.482 → 0.605 ph.u.), Ti (0.284 → 0.300 ph.u.), and Fe^{2+} (0.753 → 0.839 ph.u.). The Cr/(Cr + Al) ratio varies from 0.69 to 0.73.

It is difficult to trace the change in the composition of Cr-magnetite from the center to the edge of the crystal. In contrast to the grains of Cr-magnetites found in aillikites, a thin rim surrounding Cr-spinels represents Cr-magnetites in damtjernites. Based on X-ray elemental maps, it can be concluded that the contents of Cr and Al decrease and Fe^{3+} and Ti increase in Cr-magnetites relative to Cr-spinels.

In Ti-magnetites of damtjernites, a decrease in Cr (to 0.001 ph.u.), Al (0.22 → 0.051 ph.u.), and Mg (0.482 → 0.043 ph.u.) is observed against the background of an increase in Fe^{3+} (0.598 → 0.931 ph.u.), Ti (0.390 → 0.448 ph.u.), and Fe^{2+} (0.871 → 1.089 ph.u.).

Spinels, as well as minerals of aillikites, correspond to the Ti-magnetite trend (Figure 5) and the trend of aillikites (Trend 3) on the graphs of $Fe^{3+}/(Fe^{3+} + Al + Cr)$ vs. $Fe^{2+}/(Fe^{2+} + Mg)$ and Al–Fe^{3+}–Cr (Figure 6).

4.2. Chuktukon Complex Spinels

In the aillikites, we have identified the following types of spinels:

(1) Cr-spinel—(Mg^{2+}, Fe^{2+}) ($Cr,Al,Fe^{3+},Ti)_2O_4$;
(2) Al-spinel—(Mg^{2+}, Fe^{2+}) ($Al,Cr,Fe^{3+},Ti)_2O_4$;
(3) Mum—(Mg^{2+}, Fe^{2+}) (Fe^{3+}, Ti, Al, $Cr)_2$ O_4.

In Cr-spinels, from the center to the edge of the grain, there is generally a decrease in the content of Cr and Fe^{2+} with an increase in the content of Al, Ti, Fe^{3+}, and Mg. The Cr/(Cr + Al) ratio varies from 0.63 to 0.71.

In BSE images and in X-ray elemental maps, no pronounced boundary between Cr-spinel and Al-spinel was found. In pleonaste spinel, the contents of Al, Mg were higher than in Cr-spinel.

In Mum spinels surrounding Al-spinels, the rim size is 10–20 μm. The composition of Mum spinels shows an increase in Fe^{3+} and Ti and a decrease in Al and Cr relative to the above-described spinels (Figure 8).

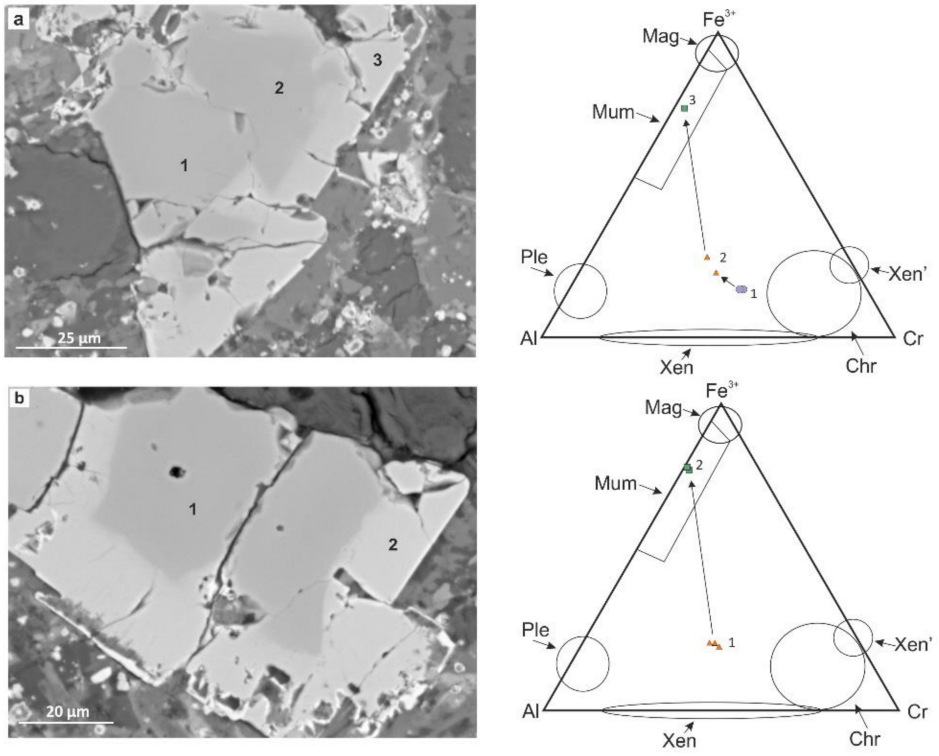

Figure 8. BSE images of zoned crystals and Al-Fe^{3+}-Cr diagrams for spinels from Chuktukon aillikites.

Most analyzed spinels fall within the Ti-magnetite trend (Trend 2 according to Mitchell (1995)), which is characteristic of Type 2 kimberlites (orangeites) and UMLs (Figure 5). However, some analyses gave results within the ulvöspinel trend in the evolution of the compositions of spinels from type I kimberlites (see Figure 5). On the Al–Fe^{3+}–Cr diagram (Figure 6b), the spinel compositions form a trend somewhat different from that of minerals from the aillikite–damtjernites of the Terina complex since their evolution starts from higher-alumina and high-chromium spinels and ends in the Mum region, not reaching Mag values.

Several types of spinels are present in damtjernites:

(1) Cr-spinels—$(Mg^{2+} \leftrightarrow Fe^{2+})$ $(Cr,Al,Fe^{3+},Ti)_2O_4$;
(2) Al-spinel—(Mg^{2+},Fe^{2+}) $(Al,Cr,Fe^{3+},Ti)_2O_4$;
(3) Cr-magnetites—(Mg^{2+},Fe^{2+}) $(Fe^{3+},Cr,Al,Ti)_2O_4$;
(4) Ti-magnetites—(Fe^{2+}, Mg^{2+}) $(Fe^{3+}, Ti, Al)_2 O_4$.

The spinel crystals from damtjernites are zonal. The Cr-spinel core is surrounded by Cr-magnetite. Atoll spinels are common. The atoll lagoon is filled with dolomite, but potassium feldspar lagoons also occur. The core of the atolls is represented by Cr-spinel, and the rim is Ti-magnetite (Figure 9).

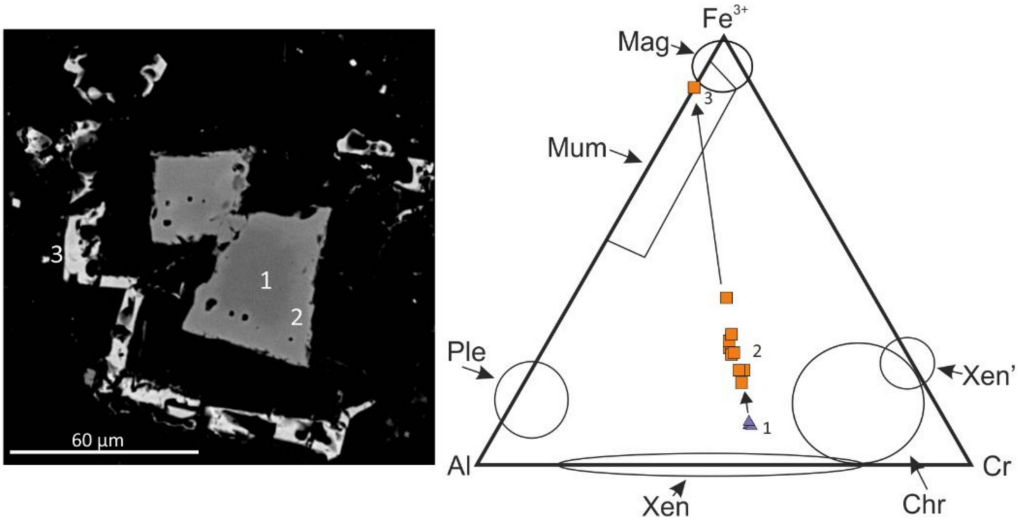

Figure 9. BSE images of crystals and diagrams Al-Fe^{3+}-Cr for spinels from Chuktukon damtjernites.

In Cr-spinels of damtjernites, the concentration of Cr is (1.011 → 0.622 ph.u.), Al (0.756 → 0.497 ph.u.), Mg (0.714 → 0.516 ph.u.), Fe^{3+} (0.250 → 0.600 ph.u.), Ti (0.107 → 0.200 ph.u.), and Fe^{2+} (0.292 → 0.603 ph.u.). The Cr/(Cr + Al) ratio varies from 0.55 to 0.69.

Al-spinels have idiomorphic crystals and are edged with Cr-spinels. Al content varies within the range 0.800–0.900 ph.u., Mg within the range 0.620–0.708 ph.u., and Fe^{2+} within the range 0.428–0.431 ph.u.

Cr-magnetites are represented by a thin rim surrounding Cr-spinels. Element maps show that Cr-magnetites are enriched in Fe and Ti and depleted in Cr and Al relative to Cr-spinels. In Ti-magnetite relative to Cr-magnetite, Cr and Mn are absent, and the content of Fe and V increases.

On the Al–Fe^{3+}–Cr diagram (Figure 6), the spinel compositions form a trend similar to that of the Chuktukon aillikites, differing in the presence of single grains of spinel xenocrystals from peridotites (Xen) and discrete compositional changes from Cr-spinel to Ti-magnetite. The same discrete quality is seen in the diagrams of Ti/(Ti + Cr + Al) vs. $Fe^{2+}/(Fe^{2+}$ + Mg) and $Fe^{3+}/(Fe^{3+}$ + Al + Cr) vs. $Fe^{2+}/(Fe^{2+}$ + Mg) (see Figures 5 and 6).

In damtjernite spinels, the Mn concentration of 0.20 wt% remains almost unchanged from Cr-spinel to Ti-magnetite. Variations in Zn (0.02–0.14 wt%) in the studied minerals depend little on the content of the main components (Cr, Al, Ti, and Fe^{3+}). The V concentration increases from Cr-spinel to Ti-magnetite (0.20 → 0.70 wt%).

4.3. Melt Inclusions Study

Primary melt inclusions were found in several grains of Cr-spinels from damtjernites of the Chuktukon complex (Figure 10). The inclusions are as large as 30 µm and are distributed without visible regularity within the grains. The melt inclusions have a complex morphology and, less often, a negative spinel shape (Figure 10). They are completely crystallized. Typical daughter phases are phlogopite (Mg # 83–91, BaO 0.7 wt%, TiO_2 2.1–5.5 wt%, F 1.1–2.3 wt%), diopside (Mg # 68–77, TiO_2 3–4 wt%), calcite or dolomite (Mg # 55–77), and apatite. Albite was diagnosed in several exposed inclusions in damtjernites. No ore phases were found in the opened inclusions, most likely due to the crystallization of Cr-spinel (host mineral) on the walls of the inclusions and, as a consequence, the consumption of Cr, Fe, and Ti from the melt.

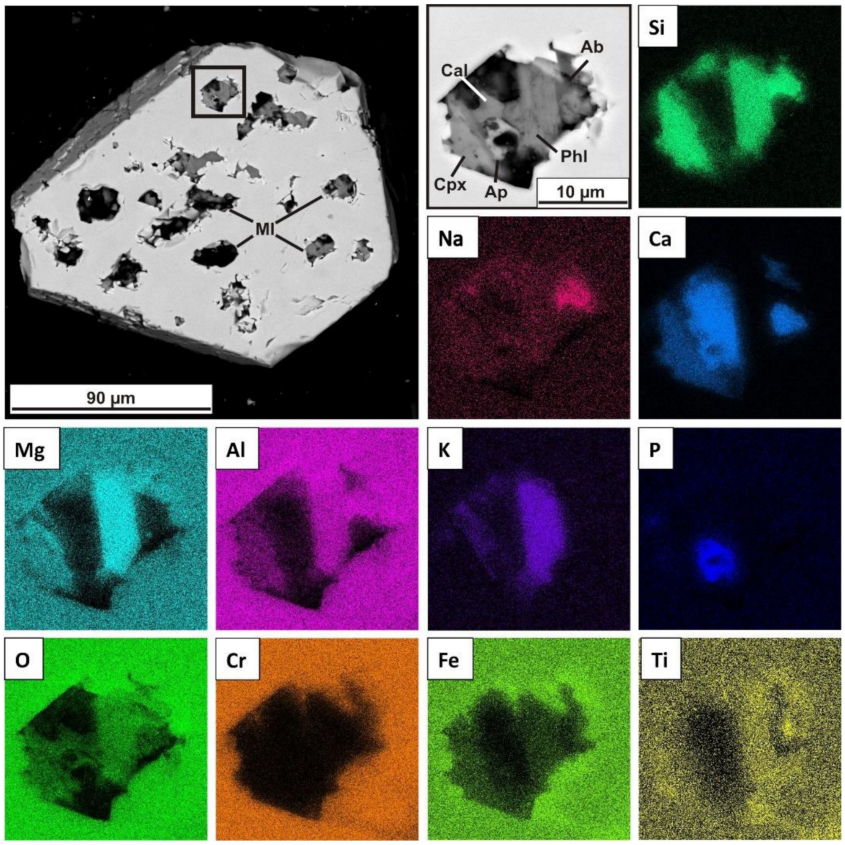

Figure 10. Melt inclusions (MI) in the Cr-spinel of the damtjernites of the Chuktukon complex, BSE images and electron microprobe (EMP) X-ray element maps. Ab—albite, Ap—apatite, Cal—calcite, Cpx—clinopyroxene, Phl—phlogopite.

5. Discussion

Primary Cr-spinels in UMLs of the Chadobets complex have a rather high Cr/(Cr + Al) ratio, reaching values of 0.75, bringing them closer to the composition of those in kimberlites (0.75–0.95) and UMLs (0.60–0.95) [27,43,44]. On the Al–Fe^{3+}–Cr diagram (Figure 6b), we can observe the main stages of spinel growth (Xen, Chr, Mum, Mag), and the main trends (1′–3′) of spinel zoning found in aillikites and damtjernites. Most of the spinels of the present study are characterized by significant changes in composition even within a single grain, which suggests rapidly changing conditions at the Chr, Mum, and Ti-Mag stages with insignificant homogenization of the spinel.

The earliest spinel grains, xenocrysts (Xen) from mantle peridotite, were found in the explosion pipes of damtjernites of the Chuktukon complex and were most likely captured during the rising of the primary melt to the surface. Reaction zones around xenocrysts formed because of interactions with the primary melt of UMLs are not pronounced and are not always diagnosed in BSE. The spinels of the aillikites and damtjernites of the Terina complex are characterized by the absence of xenogenic spinels, which could be due to the relatively slower crystallization at higher temperatures compared to the Chuktukon damtjernites (Figure 6). This could promote homogenization and/or dissolution of the xenogeneic spinels. It is worth noting that the observed variations in the composition of spinels of the Chuktukon damtjernites do not show a reactionary trend in the interaction of xenogenic spinel from peridotite with kimberlite melt (Trend 4) described by [27] (Figure 6). However, some of the spinel analyses fall within the primary chromite (Chr) fields typical for kimberlites [27].

The composition of high-chromium spinels successively changed to a high-alumina composition, and the obtained values fit into alumina Trend 3, identified by Roedder and Schulze (2008) for kimberlites and UMLs (Figure 6). Roedder and Schulze (2008) argue

that Trend 3 is parallel to the Irvine olivine and spinel isopotential curves [46] and is the result of rapid temperature changes and diffusion-controlled crystallization. Petrographic studies and the results of studying inclusions in olivine from UMLs of the Chuktukon and Terina complexes confirm this possibility [40].

Further crystallization of high-alumina Cr-spinels leads to three similar trends (Trends 1′–3′) that show a significant decrease in the amounts of Al and Cr with a change in composition from Chr to Mum (Figure 6). This change could be the result of a combination of various factors such as the degassing of magma with the release of carbon dioxide, rapid temperature changes, and crystallization of other minerals in the groundmass.

First, the crystallization of phlogopite in the UMLs of the Terina and Chuktukon complexes could be the reason for the decrease in Al in the melt. A similar tendency with crystallization of early phlogopite is observed in Group II kimberlites [27,42,47]. No less important is the presence of early carbonates in the aillikites and damtjernites of Chuktukon and Terina, which were formed during the crystallization of UMLs. In this case, carbon dioxide, which is an important component in the evolution of melts, could lead to an explosive character during the rapid rise of melts to the surface, among other things. This fact is confirmed by the presence of the damtjernite explosive tube bodies. Therefore, a sharp change in the composition from Chr to Mum (Trends 1′–3′, Figure 6) could be initiated additionally by degassing, which leads to rapid changes in the temperature and composition of the melt.

The mineralogical data on the composition of UMLs of the Chadobets complex are in full agreement with data from studies of melt inclusions in the Cr-spinels of the UMLs. This study of the chemical composition of the crystalline primary melt inclusions showed the predominance of carbonate (calcite and dolomite) and aluminosilicate daughter phases (phlogopite, clinopyroxene, and/or albite). [27] argue that in carbonate-bearing kimberlites formed under relatively oxidizing conditions, magnesium activity remained high during spinel crystallization. This fact, in their opinion, led to an almost constant and relatively low $Fe^{2+}/(Fe^{2+} + Mg)$ ratio in the spinel of Trend 1 (see Figure 6). In the spinels studied here, with the evolution of their composition from Chr to Mum, the amount of Mg and the $Fe^{2+}/(Fe^{2+} + Mg)$ ratio change insignificantly (Figure 6), which also confirms the important role of carbonates. Similar examples, where spinel contains an increased amount of magnesioferrite ($MgFe^{3+}{}_2O_4$) component, include carbonate-containing UMLs in Greenland and Canada [43,44].

Further evolution from Mum to Ti-Mag is accompanied by the formation of atoll structures. There are several points of view on the origin of the atoll texture: (1) the structure of the atoll in spinel is a sign of resorption and is formed when the previously formed spinel dissolves [18,48–50]; (2) the structure of the atoll could develop with supersaturation and rapid cruciform growth of spinel in the corners of the crystal, and the crystal faces did not have enough components to complete their growth [51]; and (3) spinel did not crystallize in the atoll lagoon due to the lack of necessary chemical components and/or the immiscibility of the spinel [27]. We suggest that the atoll texture in the present study is due to spinel resorption. The middle part of the atoll spinel may have an unstable composition as a result of rapid uplift and significant changes in fluid/melt composition at later stages. As a result, upon dissolution and replacement of Mum spinels, lagoons form, followed by the formation of the Mag rim. The mechanism of metasomatic replacement observed in atoll spinel is described in numerous works [52–57]. We suggest that replacement occurs at later stages because of fluid seepage in the intergranular space, where gas bubbles are an effective agent for transporting the reacting fluid and elements.

6. Conclusions

1. Chemical investigations of the spinel minerals of the UMLs from the Chadobets complex show the following main stages of the spinels' evolution: Xen → Cr-Spl →Mum → Ti-Mag.

2. The spinel xenocrysts (Xen) were found only in the damtjernite pipes and formed from mantle peridotite. They were captured during the rapid rising of the primary UML melt to the surface.
3. The composition of high-chromium (Cr) spinels successively changed to a high-alumina composition caused by early olivine and spinel co-crystallization. The high-alumina spinels were then transformed to magnesian ulvöspinel–magnetites with a strong decrease in the Al and Cr amounts caused by the release of carbon dioxide, rapid temperature changes, and crystallization of the main magmatic minerals in the groundmass, such as phlogopite and carbonates.
4. Melt inclusion investigation showed the predominance of carbonate (calcite and dolomite) and aluminosilicate daughter phases (phlogopite, clinopyroxene, and/or albite) that are in full agreement with the chemical evolutional Cr-spinel crystallization trend.
5. Further evolution of the spinels from Mum to Ti-Mag is accompanied by the formation of atoll structures caused by spinel resorption.

Author Contributions: Conceptualization, Y.N., A.D.; data curation, Y.N., A.D.; investigation, Y.N., I.P., A.S.; methodology, Y.N., I.P., A.D., A.S.; project administration, A.D.; writing—original draft, Y.N., A.D., I.P.; writing—review and editing, Y.N., A.D., I.P. All authors have read and agreed to the published version of the manuscript.

Funding: The investigations were supported by the Russian Science Foundation (RSF), project #19-77-10004.

Data Availability Statement: Not applicable.

Acknowledgments: Analytical equipment for this study was provided by the Analytical Center for Multi-Elemental and Isotope Research SB RAS, Novosibirsk, Russia. The work was done on state assignment of IGM SB RAS (0330-2016-0002) and GIN SB RAS (AAAA-A21-121011390002-2).

Conflicts of Interest: The authors declare no conflict of interest.

References

1. Chalapathi Rao, N.V.; Gibson, S.A.; Pyle, D.; Dickin, A.P. Petrogenesis of Proterozoic lamproites and kimberlites from the Cuddapah basin and Dharwar cratons, Southern India. *J. Petrol.* **2004**, *45*, 907–948. [CrossRef]
2. Gaffney, A.M.; Blichert-Toft, J.; Nelson, B.K.; Bizzarro, M.; Rosing, M.; Albarede, F. Constraints on source-forming processes of West Greenland kimberlites inferred from Hf-Nd isotope systematics. *Geochim. Cosmochim. Acta* **2007**, *71*, 2820–2836. [CrossRef]
3. Tappe, S.; Foley, S.F.; Kjarsgaard, B.A.; Romer, R.L.; Heaman, L.M.; Stracke, A.; Jenner, G.A. Between carbonatite and lamproite-diamondiferous Torngat ultramafic lamprophyres formed by carbonate-fluxed melting of cratonic MARID-type metasomes. *Geochim. Cosmochim. Acta* **2008**, *72*, 3258–3286. [CrossRef]
4. Bergman, S.C. Lamproites and other potassium-rich igneous rocks: A review of their occurrence, mineralogy and geochemistry. In *Alkaline Igneous Rocks*; Fitton, J.G., Upton, B.G.J., Eds.; Geological Society: London, UK, 1987; pp. 103–190.
5. Kumar, A.; Heaman, L.M.; Manikyamba, C. Mesoproterozoic kimberlites in South India: A possible link to ~1.1 Ga globalmagmatism. *Precambrian Res.* **2007**, *154*, 192–204. [CrossRef]
6. Mitchell, R.H. A review of the mineralogy of lamproites. *Trans. Geol. Soc. S. Afr.* **1985**, *88*, 411–437.
7. Mitchell, R.H.; Bergman, S.C. *Petrology of Lamproites*; Plenum Press: New York, NY, USA, 1991; 447p.
8. Mitchell, R.H. Accessory rare earth. strontium, barium and zirconium minerals in the benfontein and wesselton calcite kimberlites, South Africa. In *Kimberlites Related Rocks and Mantle Xenoliths 1*; Meyer, H.O.A., Leonardos, O.H., Eds.; CPRM Special Publication: Araxa, Brazil, 1994; pp. 115–128.
9. Mitchell, R.H. Potassic magmas derived from metasomatized lithospheric mantle: Nomenclature and relevance to exploration for diamond bearing rocks. *J. Geol. Soc. India* **2006**, *67*, 317–327.
10. Mitchell, R.H. Petrology of hypabyssal kimberlites: Relevance to primary magma compositions. *J. Volcanol. Geoth. Res.* **2008**, *174*, 1–8. [CrossRef]
11. Shoji, A.; Satoko, I. Zincian chromite inclusions in diamonds: Possibility of deep recycling origin. *J. Mineral. Petrol. Sci.* **2011**, *106*, 85–90.
12. Barnes, S.J.; Roedder, P.L. The range of spinel compositions in terrestrial mafic and ultramafic rocks. *J. Petrol.* **2001**, *42*, 2279–2302. [CrossRef]
13. Grütter, H.S.; Apter, D.B. Kimberlite and lamproite-borne chromite phenocrysts with "diamond inclusion"-type chemistries. In *Extended Abstracts, 7th International Kimberlite Conference*; University of Cape Town: Cape Town, South Africa, 1998; pp. 280–288.

14. Jaques, A.L. Major and trace element variations in oxide and titanate minerals in the West Kimberley lamproites, Western Australia. *Mineral. Petrol.* **2016**, *110*, 159–197. [CrossRef]
15. Kamenetsky, V.M.; Crawford, A.J.; Meffre, S. Factors controlling chemistry of magmatic spinel: An empirical study of associated olivine, Cr-spinel and melt inclusions from primitive rocks. *J. Petrol.* **2001**, *42*, 655–671. [CrossRef]
16. Klemme, S. The influence of Cr on the garnet–spinel transition in the Earth's mantle: Experiments in the system MgO–Cr_2O_3–SiO_2 and thermodynamic modeling. *Lithos* **2004**, *77*, 639–646. [CrossRef]
17. Haggerty, S.E. The chemistry and genesis of opaque minerals in kimberlite. In *Physics and Chemistry of the Earth*; Ahrens, L.H., Dawson, J.B., Duncan, A.R., Erlank, A.J., Eds.; Pergamon Press: Oxford, UK, 1975; Volume 9, pp. 295–307.
18. Mitchell, R.H. *Kimberlites: Mineralogy, Geochemistry, and Petrology*; Plenum Press: New York, NY, USA, 1986; 442p.
19. Kamenetsky, V.S.; Golovin, A.V.; Maas, R.; Giuliani, A.; Kamenetsky, M.B.; Weiss, Y. Towards a new model for kimberlite petrogenesis: Evidence from unaltered kimberlites and mantle minerals. *Earth Sci. Rev.* **2014**, *139*, 145–167. [CrossRef]
20. Kargin, A.V.; Sazonova, L.V.; Nosova, A.A.; Lebedeva, N.M.; Tretyachenko, V.V.; Abersteiner, A. Cr-rich clinopyroxene megacrysts from the Grib kimberlite, Arkhangelsk province, Russia: Relation to clinopyroxene–phlogopite xenoliths and evidence for mantle metasomatism by kimberlite melts. *Lithos* **2017**, *292–293*, 34–48. [CrossRef]
21. Krmíček, L.; Romer, R.L.; Ulrych, J.; Glodny, J.; Prelević, D. Petrogenesis of orogenic lamproites of the bohemian massif: Sr–Nd–Pb–Li isotope constraints for Variscan enrichment of ultradepleted mantle domains. *Gondwana Res.* **2016**, *35*, 198–216. [CrossRef]
22. Kubínová, Š.; Faryad, S.W.; Verner, K.; Schmitz, M.; Holub, F. Ultrapotassic dykes in the Moldanubian zone and their significance for understanding of the post-collisional mantle dynamics during Variscan orogeny in the bohemian massif. *Lithos* **2017**, *272–273*, 205–221. [CrossRef]
23. Jaques, A.L.; Lewis, J.D.; Smith, C.B. The kimberlites and lamproites of Western Australia. *Geol. Surv. West. Aust. Bull.* **1986**, *132*, 65.
24. Rimsaite, J. Distribution of major and minor constituents between mica and host ultrabasic rocks, and between zoned mica and zoned spinel. *Contrib. Mineral. Petrol.* **1971**, *33*, 259–272. [CrossRef]
25. Schulze, D.J. Origins of chromian and aluminous spinel macrocrysts from kimberlites in southern Africa. *Can. Mineral.* **2001**, *39*, 361–376. [CrossRef]
26. Su, B.X.; Zhang, H.F.; Sakyi, P.A.; Yang, Y.-H.; Ying, J.-F.; Tang, Y.-J.; Qin, K.-Z.; Xiao, Y.; Zhao, X.-M.; Mao, Q.; et al. The origin of spongy texture in minerals of mantle xenoliths from the Western Qinling, Central China. *Contrib. Mineral. Petrol.* **2011**, *161*, 465–482. [CrossRef]
27. Roeder, P.L.; Schulze, D.J. Crystallization of groundmass spinel in kimberlite. *J. Petrol.* **2008**, *49*, 1473–1495. [CrossRef]
28. Tappe, S.; Foley, S.F.; Jenner, G.A.; Kjarsgaard, B.A. Integrating ultramafic lamprophyres into the IUGS classification of igneous rocks: Rational and implications. *J. Petrol.* **2005**, *46*, 1893–1900. [CrossRef]
29. Doroshkevich, A.G.; Chebotarev, D.A.; Sharygin, V.V.; Prokopyev, I.R.; Nikolenko, A.M. Petrology of alkaline silicate rocks and carbonatites of the Chuktukon massif, Chadobets upland, Russia: Sources, evolution and relation to the Triassic Siberian LIP. *Lithos* **2019**, *332–333*, 245–260. [CrossRef]
30. Lapin, A.V. About kimberlites of the Chadobets upland in connection with a problem of the formational-metallogeny analysis of the platform alkaline ultrabasic magmatic rocks. *Otechestvennaya Geol.* **2001**, *4*, 30–35. (In Russian)
31. Nosova, A.A.; Kargin, A.V.; Sazonova, L.V.; Dubinina, E.O.; Chugaev, A.V.; Lebedeva, N.M.; Yudin, D.S.; Larionova, Y.O.; Abersteiner, A.; Gareev, B.I. Sr-Nd-Pb isotopic systematic and geochronology of ultramafic alkaline magmatism of the southwestern margin of the Siberian Craton: Metasomatism of the sub-continental lithospheric mantle related to subduction and plume events. *Lithos* **2020**, *364–365*, 105509. [CrossRef]
32. Chebotarev, D.A.; Doroshkevich, A.G.; Klemd, R.; Karmanov, N.S. Evolution of Nbmineralization in the Chuktukon carbonatite massif, Chadobets upland (Krasnoyarsk Territory, Russia). *Period. Mineral.* **2017**, *86*, 99–118. [CrossRef]
33. Dashkevich, N.N. Regional prediction of kimberlite magmatism in the southwestern Siberian Platform. In *Geologiya i poleznye iskopaemye Krasnoyarskogo kraya (Geology and Mineral Resources of Krasnoyarsk District)*; Krasnoyarsk Book Publishing House: Krasnoyarsk, Russia, 1999; pp. 31–42. (In Russian)
34. Lapin, A.V.; Lisitzyn, D.V. About mineralogical typomorphism of alkaline ultrabasic magmatic rocks of Chadobets upland. *Otechestvennaya Geol.* **2004**, *683*, 93. (In Russian)
35. Lapin, A.V.; Pyatenko, I.K. Chadobets complex of ultrabasic alkaline rocks and carbonatites: New data about composition and condition of formation. *Dokl. Earth Sci.* **1992**, *6*, 88–101. (In Russian)
36. Lomayev, V.G.; Serdyuk, S.S. The Chuktukon Nb-TR deposit—The priority object for modernization of the Russian rare-earth industry. *J. Sib. Fed. Univ.* **2011**, *4*, 132–154.
37. Kirichenko, T.; Zuev, K.; Perfilova, O.Y.; Sosnovskaya, O.; Smokotina, I.; Markovich, L.A.; Borodin, M.E. *State Geological Map of Russian Federation, Scale 1: 1000000 (Third Generation)*; Angaro-Eniseysky series; Sheet O-47 Bratsk. Explanatory Note; Cartografic Factory of VSEGEI: St. Petersburg, Russia, 2012; pp. 163–179. (In Russian)
38. Chebotarev, D.A.; Doroshkevich, A.G.; Sharygin, V.V.; Yudin, D.S.; Ponomarchuk, A.V.; Sergeev, S.A. Geochronology of the Chuktukon carbonatite massif, Chadobets uplift (Krasnoyarsk Territory). *Russ. Geol. Geophys.* **2017**, *58*, 1222–1231. [CrossRef]

39. Doroshkevich, A.G.; Sharygin, V.V.; Belousova, E.A.; Izbrodin, I.A.; Prokopyev, I.R. Zircon from the Chuktukon alkaline ultramafic carbonatite complex (Chadobets uplift, Siberian craton) as evidence of source heterogeneity. *Lithos* **2021**, *382–383*, 105957. [CrossRef]
40. Prokopyev, I.; Starikova, A.; Doroshkevich, A.; Nugumanova, Y.; Potapov, V. Petrogenesis of Ultramafic Lamprophyres from the Terina Complex (Chadobets Upland, Russia): Mineralogy and Melt Inclusion Composition. *Minerals* **2020**, *10*, 419. [CrossRef]
41. Bosi, F.; Biagioni, C.; Pasero, M. Nomenclature and classification of the spinel supergroup. *Eur. J. Mineral.* **2019**, *31*, 183–192. [CrossRef]
42. Mitchell, R.H. *Kimberlites, Orangeites and Related Rocks*; Plenum Press: New York, NY, USA, 1995; 410p.
43. Tappe, S.; Foley, S.F.; Jenner, G.A. Genesis of ultramafic lamprophyres and carbonatites at Aillik Bay, Labrador: A consequence of incipient lithospheric thinning beneath the North Atlantic craton. *J. Petrol.* **2006**, *47*, 1261–1315. [CrossRef]
44. Upton, B.G.J.; Craven, J.A.; Kirstein, L.A. Crystallisation of mela-aillikites of the Narsaq region, Gardar alkaline province, south Greenland and relationships to other aillikitic–carbonatitic associations in the province. *Lithos* **2006**, *92*, 300–319. [CrossRef]
45. Roeder, P.L.; Poustovetov, A.; Oskarsson, N. Growth forms and composition of chromian spinel in MORB magma: Diffusioncontrolled crystallization of chromian spinel. *Can. Mineral.* **2001**, *39*, 397–416. [CrossRef]
46. Irvine, T.N. Chromian spinel as a petrogenetic indicator. Part, I. Theory. *Can. J. Earth Sci.* **1965**, *2*, 648–672. [CrossRef]
47. Pasteris, J.D. Spinel zonation in the De beers kimberlite, South Africa: Possible role of phlogopite. *Can. Mineral.* **1983**, *21*, 41–58.
48. Carpenter, R.L.; Edgar, A.D.; Thibault, Y. Origin of spongy textures in clinopyroxene and spinel from mantle xenoliths, hessian depression, Germany. *Mineral. Petrol.* **2002**, *74*, 149–162. [CrossRef]
49. Kumar, S.P.; Shaikh, A.M.; Patel, S.C.; Sheikh, J.M.; Behera, D.; Pruseth, K.L.; Ravi, S.; Tappe, S. Multi-stage magmatic history of olivine–leucite lamproite dykes from Banganapalle, Dharwar craton, India: Evidence from compositional zoning of spinel. *Mineral. Petrol.* **2020**, *115*, 87–112. [CrossRef]
50. Streck, M.J. Mineral textures and zoning as evidence for open system processes. *Rev. Mineral. Geochem.* **2008**, *69*, 595–622. [CrossRef]
51. Armstrong, K.A.; Roeder, P.L.; Helmstaedt, H.H. Composition of spinels in the C14 kimberlite, Kirkland Lake, Ontario. *Russ. Geol. Geophys.* **1997**, *38*, 454–466.
52. Putnis, A. Mineral replacement reactions: From macroscopic observations to microscopic mechanisms. *Mineral. Mag.* **2002**, *66*, 689–708. [CrossRef]
53. Putnis, A. Mineral replacement reactions. *MSA Rev. Mineral. Geochem.* **2009**, *70*, 87–124. [CrossRef]
54. Putnis, C.V.; Mezger, K. A mechanism of mineral replacement: Isotope tracing in the model system KCl-KBr-H2O. *Geochim. Cosmochim. Acta* **2004**, *68*, 2839–2848. [CrossRef]
55. Putnis, C.V.; Tsukamoto, K.; Nishimura, Y. Direct observations of pseudomorphism: Compositional and textural evolution at a fluid-solid interface. *Am. Mineral.* **2005**, *90*, 1909–1912. [CrossRef]
56. Watson, E.B.; Brenan, J.M. Fluids in the lithosphere, 1. Experimentally-determined wetting characteristics of CO2-H2O fluids and their implications for fluid transport, host-rock physical properties and fluid inclusion formation. *Earth Planet. Sci. Lett.* **1987**, *85*, 497–515. [CrossRef]
57. Watson, E.B.; Brenan, J.M.; Baker, D.R. Distribution of fluids in the mantle. In *Continental Mantle*; Menzies, M.A., Ed.; Clarendon: Oxford, UK, 1990.